Volume 1 | Number 1 | Jan 2013 | Pages 1–100

Soft Matter

www.rsc.org/softmatter

ROYAL SOCIETY OF CHEMISTRY

ROYAL SOCIETY OF CHEMISTRY

www.rsc.org/softmatter

Microphase separation of short wormlike diblock copolymers with finite interaction range

Ying Jiang[1], Xinghua Zhang[2],* Bing Miao[3],* Dadong Yan[4], and

Jeff Z. Y. Chen[5]

[1]*School of Chemistry and Environment, Center of Soft Matter Physics and its Applications,*

Beihang University, Beijing 100191, China,

[2]*School of Science, Beijing Jiaotong University, Beijing 100044, China,*

[3]*College of Materials Science and Opto-Electronic Technology, University of Chinese Academy of*

Sciences, Beijing 100049, China,

[4]*Department of Physics, Beijing Normal University, Beijing 100875, China,*

[5]*Department of Physics and Astronomy,*

University of Waterloo, Waterloo, Ontario, Canada N2L 3G1

E-mail: zhangxh@bjtu.edu.cn; bmiao@ucas.ac.cn

Abstract

We investigate several structural properties of low-molecular weight AB diblock copoly-
mer melts, focusing on a number of features that substantially deviate from those of high-
molecular weight copolymer melts. The study is based on the wormlike chain formalism
aided by random phase approximation and self-consistent field theory. We examine the effect-
s stemmed from both finite molecular wight and finite interaction range between unlike AB
monomers. The latter yields profound effects on systems consisting of short wormlike block

---

*To whom correspondence should be addressed

copolymers. Noticeable shift of the order-disorder transition point is discussed. Attention is also paid to the strong-segregation regime, where low molecular weight polymers are subject to finite stretchability.

I. Introduction

Micro-phase separated low-molecular-weight AB diblock copolymers have drawn considerable experimental attention recently. Exciting new technological applications of these systems, such as block copolymer lithography,[1,2] have been actively pursued. For example, by reducing the molecular weight, sub-20 nm domain features can now be achieved.[3–7] In another class of problems, from the view of coarse graining, short amphiphilic molecules such as surfactant and lipid molecules are usually modeled by short polymers, both experimentally and theoretically for nanotechnological and biological applications.[8–12]

The nature of the ordered structures in a high-molecular-weight diblock copolymer melt depends on a number of essential parameters. The combination χN is known as an important parameter which derive the system to phase-separate, where χ is the Flory-Huggins prameter and N is the degree of polymerization. The volume fraction of a component f (for example the A-component) is more important in determining the type of the ordered structures. Over the entire χN-f phase diagram these two parameters collectively capture the basic phase behavior.[13,14] A self consistent field theory (SCFT) can be developed based on the Edwards weight,[15,16] also known as a Gaussian-chain (GSC) model, as the statistical weight describing the chain configuration of polymers. Notably N appears in the combination χN and is not an independent parameter in such a model. For a detailed review please refer to Refs.[17–19]

One distinctive new feature of a low-molecular-weight system is the introduction of N as an additional parameter. Physically, a small-N system no longer has the coil conformation entropy that can usually be associated with a random walk. The relatively persistent conformation has a lower conformation entropy in comparison with a coil conformation with the same total polymer length;

it hence allows the phase separation at a lower χN. To account for the finite-N effects, a SCFT formalism can be established based on the wormlike model for a semiflexible polymer.[20,21] After identifying the persistence length λ with the effective Kuhn length a by $a = 2\lambda$, such a formalism reduces to the Gaussian-chain SCFT in the asymptotic limit $N \gg 1$ and retains the finite N as an independent parameter in other parameter regimes. The lowering of the order-disorder transition point of a finite N system, for example, is correctly described in such a theory.[22–24] Currently a SCFT phase diagram for wormlike AB diblock copolymer melts as a function of three parameters, $f, \chi N$ and N, is available.[25,26] A brief summary of the theory is given here in Appendix B.

All these developments incorporated the classical Flory-Huggins energy for the description of the enthalpy penalty of mixing unliking A and B monomers. The basic assumption behind such a energy form is that the A/B interaction has a local form, i.e., the interaction range is much shorter than the Kuhn length. Matsen recently questioned this basic assumption by introduction of a finite force range ε.[27] The ratio ε/a becomes another parameter in SCFT. A SCFT study based on the model of freely jointed diblock copolymer chain was carried out and it demonstrated the need of incorporating the finite ε/a effects, particularly for low molecular weight systems.[27]

The distance-dependent interaction proposed in the present work to study the stability of phase transitions of diblock copolymer melts originates from the consideration that the finite volume of the coarse-grained segment usually consists of several tens of monomers in real systems.[19,28] It plays a significant role in phase separations of short block copolymers. Phenomenologically, we take into account the volume of each segment directly by distributing the mass of the segments over a finite volume (assumed Gaussian)[29] rather than treating them as mass points. One benefit of this coarse-graining approach is that the resulting field theory contains a well-behaved continuum limit which is free of ultraviolet (UV) divergence resulted from the commonly-used Edwards delta function potential as the collocation grid is further refined.[30] More recently, this technique has been successfully utilized in field theory simulations in a variety of polymeric systems, such as the complex coacervate-forming system,[31] polymer nanocomposites[32,33] and polymer solutions.[34]

In this paper, we analyze a number of potentially important structural properties of a wormlike

diblock copolymer melt, incorporating the finite interaction range. A complete analysis in the entire four-parameter space, χN, f, N, and ε/a, is too complicated. Instead, we primarily explore features that are unique to this system. The theoretical problem is defined in Sect. II.

To start with, in Sect. III A, we visit the change of the spinodal point $(\chi N)_s$ at $f = 1/2$ for a womrlike diblock copolymer containing finite force range, from the classical value 10.495... for a flexible diblock copolymer system. To achieve this we follow the method of random phase approximation (RPA), which enables us to determine $(\chi N)_s$ as a function of N and ε/a at $f = 1/2$. As will be shown below, smaller-N yields lowering of $(\chi N)_s$ and finite-ε/a produces raising of $(\chi N)_s$. At $f = 1/2$ and beyond $(\chi N)_s$, the system enters into a lamella ordered state. The effects of finite N and ε/a on the domain size are discussed in Sect. III B. The basic RPA formalism for the current system is reviewed in Appendix A and the numerical procedure can be found in Ref.[24]

We move to the discussion of the strongly segregation regime of a $f = 1/2$ and $\varepsilon/a = 0$ system in Sect. III C. For a flexible diblock copolymer system, this is the regime where strong-segregation theory can be applied;[35,36] the reduced interfacial width between A- and B-rich regions and lamella domain size, for example, were predicted to follow specific power laws as a function of χN. The unbounded stretching of the elastic spring assumed in a Gaussian-chain model arises subject to strong external fields.[37] This unphysical feature is corrected in a wormlike-chain model. The interfacial width and lamella domain size in a low-N system are shown to substantially deviate from those ideal power laws. The calculation of these properties, now beyond the spinodal point, is dependent on a wormlike chain SCFT; a summary of which is presented in Appendix B.

Then, still at $f = 1/2$ but for three specific examples of $\chi = 0.5$, 1, and 2, we consider the properties of the finite force range ($\varepsilon/a \neq 0$) in the strong-segregation regime of wormlike copolymers in Sect. III D . Both interfacial width and lamella domain size are used to illustrate properties of a finite ε/a.

Finally, taking $N = 10$, in Sect. III E, we present the phase diagram in the traditional χN-f view for low molecular weight wormlike diblock copolymers, at three separate values of ε/a, 0, 0.2 and 0.4. Overall, the ordered state, body-centered cubic, hexagonal, gyroid, and lamella, predicted

from a theory with $N \gg 1$ and $\varepsilon/a = 0$ are found still stable. The entire ordered phase region of a nonzero ε/a system is shown to consistently shift up from the ordered phase region of a $\varepsilon/a = 0$ system.

II. Theoretical formalism

In this section, we review the basic formalism of semiflexible AB diblock copolymers, on the basis of the continuum wormlike-chain (WLC) model. An emphasis is placed on introducing the finite force range ε in the theory.

We consider a system of n monodisperse diblock copolymer chains, each having two connected linear blocks, A and B, of different contour lengths L_A and L_B. For simplicity, the same persistence length λ is assumed for both A and B blocks. This bare persistence length is identified here with an effective Kuhn length $a \equiv 2\lambda$ so that the WLC formalism reduces to the GSC formalism in the flexible limit.[21] The same monomeric volume $1/\rho_0$ is assumed for both blocks and the volume fraction of the A blocks can be identified by $f = L_A/L$ where L is the total polymer length.

The configuration of the kth polymer chain is described by a space curve $\mathbf{R}_k(t)$, in which t is an arc variable along the curve continuously varying from one end ($t = 0$) to another one ($t = 1$). According to the Saito-Takahashi-Yunoki (STY) model,[21] the reduced total bending energy of wormlike chains of the system can be written as

$$\beta\mathcal{H}_0 = \frac{a}{4L} \sum_{k=1}^{n} \int_0^1 dt \left| \frac{d\mathbf{u}_k(t)}{dt} \right|^2, \tag{1}$$

where β is the Boltzmann factor. The unit tangent vector $\mathbf{u}_k(t) \equiv (1/L)d\mathbf{R}_k(t)/dt$ specifies the local orientation of the kth polymer chain at location t. The conformational properties of a polymer in free space described by this model depends on the ratio L/a. In the long-chain limit, this ratio is simply the number of monomers that is usually denoted by N.

The immiscibility between AB monomers is modeled by an enthalpic penalty. For a particular

system configuration, the A and B monomer fractions are defined by

$$\hat{\phi}_A(\mathbf{r}) \equiv \frac{N}{\rho_0} \sum_{k=1}^{n} \int_0^f dt \delta(\mathbf{r} - \mathbf{R}_k(t)) \tag{2}$$

$$\hat{\phi}_B(\mathbf{r}) \equiv \frac{N}{\rho_0} \sum_{k=1}^{n} \int_f^1 dt \delta(\mathbf{r} - \mathbf{R}_k(t)). \tag{3}$$

Matsen[27] revisited a more general form for the mixing enthalpy,

$$\beta H_1 = \chi \rho_0 \int d\mathbf{r} \int d\mathbf{r}' h(\mathbf{r} - \mathbf{r}') \hat{\phi}_A(\mathbf{r}) \hat{\phi}_B(\mathbf{r}'), \tag{4}$$

which has a form that is originally suggested by Helfand.[16] A classical treatment is to write the

kernel function $h(\mathbf{r})$ in a local form, in terms of the Dirac delta function $h(\mathbf{r}) = \delta(\mathbf{r})$. This leads to

the Flory-Huggins enthalpy frequently used in polymer theories.[38]

   Other forms of the function $h(\mathbf{r})$ can be used to represent finite interaction force range. For

convenience, we assume that $h(\mathbf{r})$ is normalized

$$\int d\mathbf{r}\, h(\mathbf{r}) = 1, \tag{5}$$

so that χ represents the net interaction arising from the two components. In this paper, we mainly

use the Gaussian function

$$h_G(\mathbf{r}) = \frac{1}{(2\pi)^{3/2} \varepsilon^3} \exp\left(-\frac{r^2}{2\varepsilon^2}\right) \tag{6}$$

which was also adopted by Matsen recently.[27] For comparison we also use the Yukawa function

$$h_Y(\mathbf{r}) = \frac{1}{4\pi \varepsilon^2 r} \exp\left(-\frac{r}{\varepsilon}\right) \tag{7}$$

where $r = |\mathbf{r}|$. The Yukawa potential is typically used to characterize the screening effects on the

pairwise interaction, such as in a polymer solution with high concentration and in a polyelectrolyte

system.[39] In both cases, ε is a characteristic interaction range. Note that ε is not the effective

interaction range defined through the second moment $\int d\mathbf{r}\, r^2 h(\mathbf{r})$; there was a minor inconsistency in Ref. [27]

III. Results and discussion

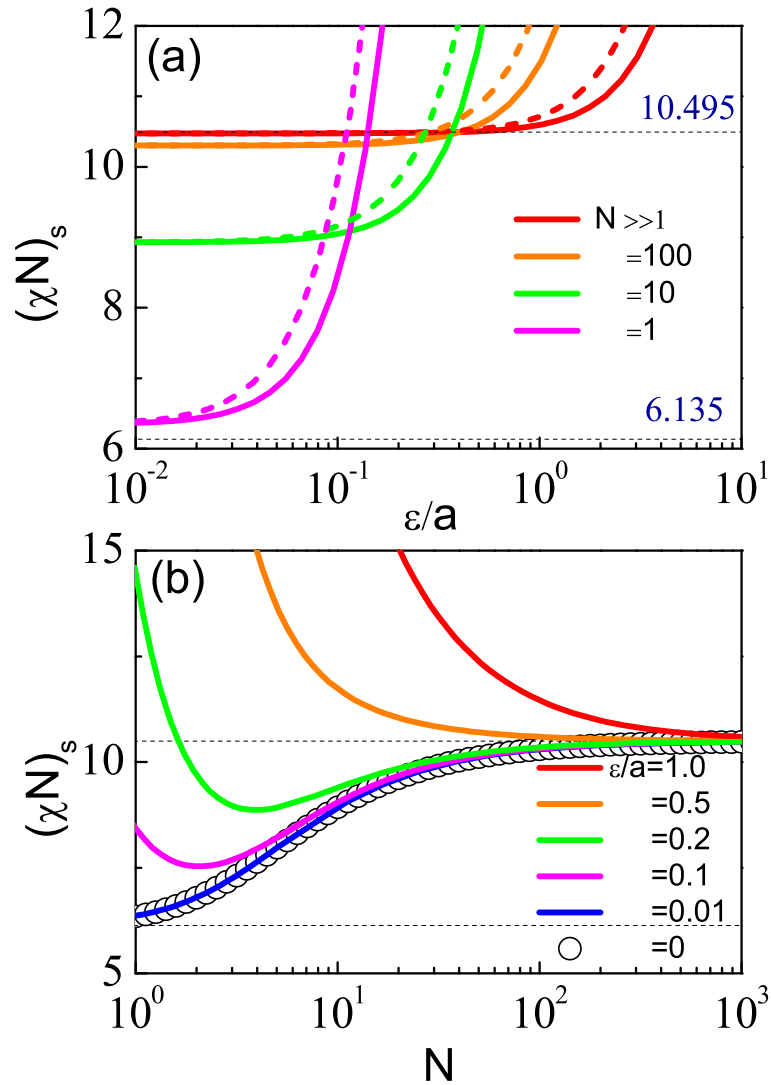## III A. Effects on spinodal lines

Figure 1: Effects of interaction range on the spinodal curve of wormlike diblock copolymer as functions of (a) the interaction range ε/a and (b) the degree of polymerization N. In (a), intermediate cases for various N are displayed here, between the flexible (large-N) and rodlike (small-N) limits. Solid and long-dashed curves represent the numerical results for the Gaussian and Yukawa interaction functions, respectively. In (b), some cases for interaction ranges as indicated are shown.

The system parameters for describing wormlike AB block copolymers are χN, N, and f. In addition, here we have the fourth parameter ε/a. Following the random-phase approximation, we can determine the stability limit of the homogeneous phase against microphase separation, which divides the weak inhomogeneous regime from homogeneous regime.

In Appendix A, we list the main RPA steps needed to calculate the spinodal point for wormlike AB diblock copolymers with a finite interaction kernel $h(\mathbf{r})$. As it turns out, the χN value at the spinodal point, $(\chi N)_s$, is determined by

$$(\chi N)_s = \min[\tilde{C}(k)/\tilde{h}(k)], \tag{8}$$

where the function in the brackets needs to be minimized with respect to the variable k. The expression of the $\mathbf{k}$-space correlation function $\tilde{C}(k)$, given in Eq. (20), is independent of ε and is no-different from the one determined from a theory without the finite interaction range consideration when $\varepsilon = 0$. This is the case where the Fourier transformation of $h(\mathbf{r})$, $\tilde{h}(k)$, has a value identical to 1, according to Eqs. (17) and (18). For WLC model, the computation of $\tilde{C}(k)$, hence $(\chi N)_s$ at $\varepsilon = 0$, was carried out in Ref.,[24] as a function of χN, N, and f. In particular, after taking the limit $N \gg 1$, we recovered the classical result, $(\chi N)_s = 10.495...$ for polymer melts made of Gaussian like chains at $f = 1/2$, first determined by Leibler.[40] On the other hand, after taking the limit $N \ll 1$, we determined $(\chi N)_s = 6.135...$ for polymer melts made of rodlike chains at $f = 1/2$, originally determined from SCFT in Refs.[22,23] These limits are indicated in Fig. 1 by dotted lines.

Fig. 1(a) is a plot of $(\chi N)_s$ as a function of ε/a for different cases of N, all at $f = 1/2$. Solid and long dashed curves represent the spinodal curves based on $h_G(\mathbf{r})$ and $h_Y(\mathbf{r})$ in Eqs. (6) and (7). While both have a similar behavior, the dashed curve increases faster than the solid curve. This is caused by the fact that for the same ε/a, the Yukawa function (exponential decay of r) has somewhat longer force range than the Gaussian function (exponential decay of r^2).

For a system composed of extremely long polymers ($N \gg 1$), there is an asymptotic curve in Fig. 1(a), which is represented by the red curve. The variation of the spinodal point is independent

of (the large) N and the correction to $(\chi N)_{\mathrm{s}} = 10.495...$ becomes significant only in the regime beyond $\varepsilon/a \sim 1$. This asymptotic limit can be inferred from Eq. (8), where $\tilde{C}(k)$ has a large-N limit and $\tilde{h}(k)$ is N-independent. Hence for systems consisting of long polymers, when the interaction range ε is smaller than the Kuhn length a, the effects of the finite force range almost vanish. A theory based on the Gaussian chain model and the original Flory-Huggins interaction is a good approximation.

The correction to $(\chi N)_{\mathrm{s}}$ due to ε/a in the mid- to short-chain parameter regime is most profound. This can be demonstrated by curves in Fig. 1(a) representing systems composed of polymers with polymerization index $N = 100, 10$ and 1 or curves in Fig. 1(b) for the variation of $(\chi N)_{\mathrm{s}}$ as a function of N at given $\varepsilon/a = 1, 0.5, 0.2, 0.1$, etc. There are two main competing effects here: finite force range and chain persistency. According to a wormlike chain theory without the finite force range effect, the latter lowers $(\chi N)_{\mathrm{s}}$,[22,24,25] as demonstrated by circles in Fig. 1(b). The finite force range, however, has an opposite effect. Within the reasonable parameter regime $\varepsilon/a \sim [0.1, 1]$, this effect prevails. The value of $(\chi N)_{\mathrm{s}}$ is now significantly altered and raises above the classical limit $(\chi N)_{\mathrm{s}} = 10.495...$ This can happen in "low" molecular weight system. The case of $N = 100$, for example, is already "low" enough to display a $(\chi N)_{\mathrm{s}}$ that deviates from the classical limit.

Instead of the wormlike chain model, the freely jointed chain (FJC) model[39] has been utilized to describe the variation of chain conformations due to finite-N effects.[27,41] Singh et al[41] used the model to determine the spinodal point through an RPA analysis. In the long-chain limit, $N \gg 1$, the location of the spinodal point $(\chi N)_{\mathrm{s}} = 10.45...$ is in agreement with Leibler's classical result at $f = 1/2$.[40] Their estimate for rod-like chains gave rise to $(\chi N)_{\mathrm{s}} = 8.3...$ which significantly differs from $(\chi N)_{\mathrm{s}} = 6.135...$ based on WLC model at $f = 1/2$.[22,24] It is worthwhile noting that the rigid rod limit in Ref.[41] referred to a diblock copolymer composed of two rigid blocks connected by a freely rotating joint. While within the present model the rod-like limit describes one rigid rod simply divided into two parts without bending. As a consequence, the conformational entropy of FJC is larger than that in the current model. Hence, its spinodal point ($\chi N = 8.3...$) is higher than that of WLC ($\chi N = 6.135...$). Matsen recently used FJC to study the finite force-range effect on

the basis of a SCFT analysis.[22] Rather than the spinodal point, he emphasized on the discussion of domain size.

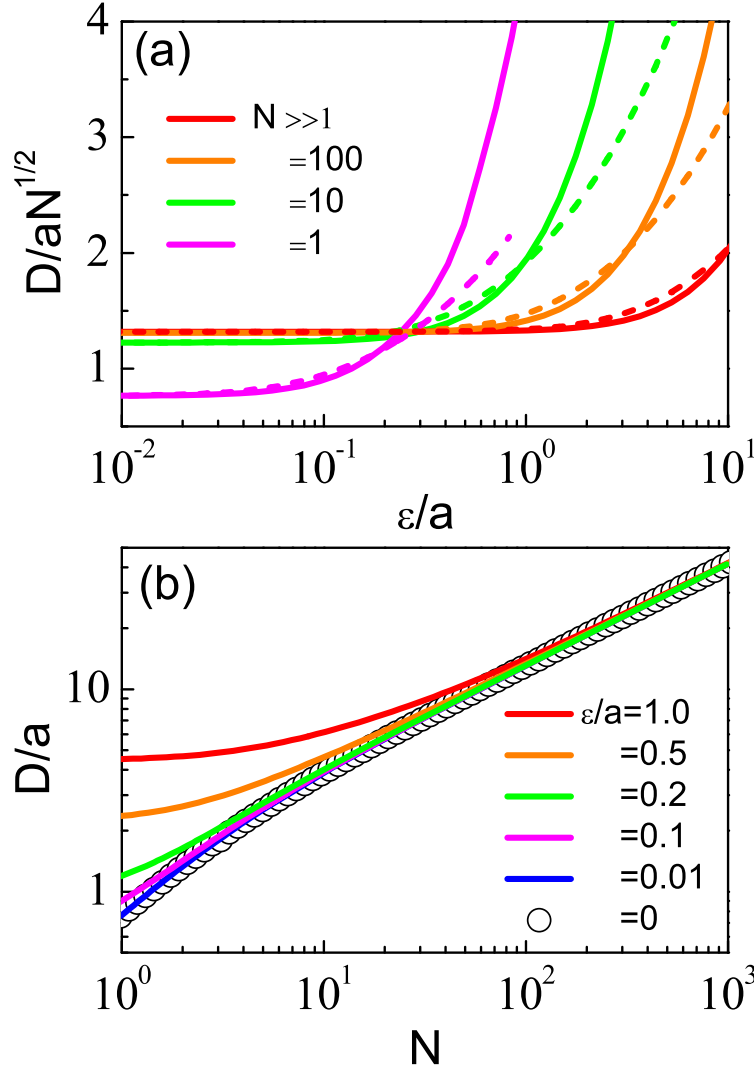## III B. Effects on lamella domain size at the phase-separation point

Figure 2: The domain size of the ordered microstructures formed by the symmetric diblock copolymers as functions of (a) the interaction range ε/a and (b) the degree of polymerization N. In (a), the solid and long-dashed curves represent the numerical results for the Gaussian and Yukawa interaction functions, respectively.

To demonstrate the N dependence of effect of interaction range, the domain size, D/a, of the ordered lamella structure formed at the microphase separation, is plotted in Fig. 2 in both

perspectives. These curves are determined from

$$D/a = k^*a, \tag{9}$$

where k^* is the optimal k that determines the minimum in Eq. (8). A symmetric diblock copolymer melt, $f = 1/2$, is considered here.

The low ε/a limit of plot (a) of the $N \gg 1$ case represents the ideal case which corresponds to a large molecular weight system with zero interaction range. In such a case $D/aN^{1/2} = 1.318$, a value that has been determined before.[40] The numerical results show that when $N \gg 1$, the finite-ε/a effects take place when $\varepsilon/a \gtrsim 1$. When N is in a relatively short range, $N \sim 10$, the finite ε/a effects become very significant in the neighborhood of $\varepsilon/a \sim 1$.

The circles in Fig. 2(b) demonstrate the $\varepsilon/a = 0$ case. The finite N effects of the domain size crosses over from the $\sim N^{1/2}$ behavior at large N to the $\sim N$ behavior at small N. Overall, a smaller-N system lowers the ratio $D/aN^{1/2}$. The finite ε/a has an opposite effect, raising D/a; in a moderate N system, it can yield a D/a that is beyond $D/aN^{1/2} = 1.318$ of an ideal case. The properties described here are consistent with the analysis based on the spinodal point in the last subsection.

Physically, near the phase-separation point, various fluctuations start to perturb the otherwise homogenously mixed state. In particular, the fluctuations near k^* dominate and that eventually bring the system to settle down at a phase-separated lamella phase for $f = 1/2$. The ideal Flory-Huggins interaction is based on mixing-AB enthalpy at a overlapping monomer physical picture ($\varepsilon/a = 0$); in finite force range system ($\varepsilon/a \neq 0$), the magnitude of this enthalpy relatively decreases from the ideal case due to the non-contact condition. The decrease depends on the wavelength of the component volume-fraction fluctuations. The dominating k^* corresponds to a wavelength $2\pi/k^*$ which is the domain size at the phase separation point. Using this wavelength for r in both Eqs. (6) and (7), we can see how the mixing entropy is reduced by an examination of Eq. (4). This effect becomes more transparent in k-space. The mixing entropy, now represented by the last term in Eq.
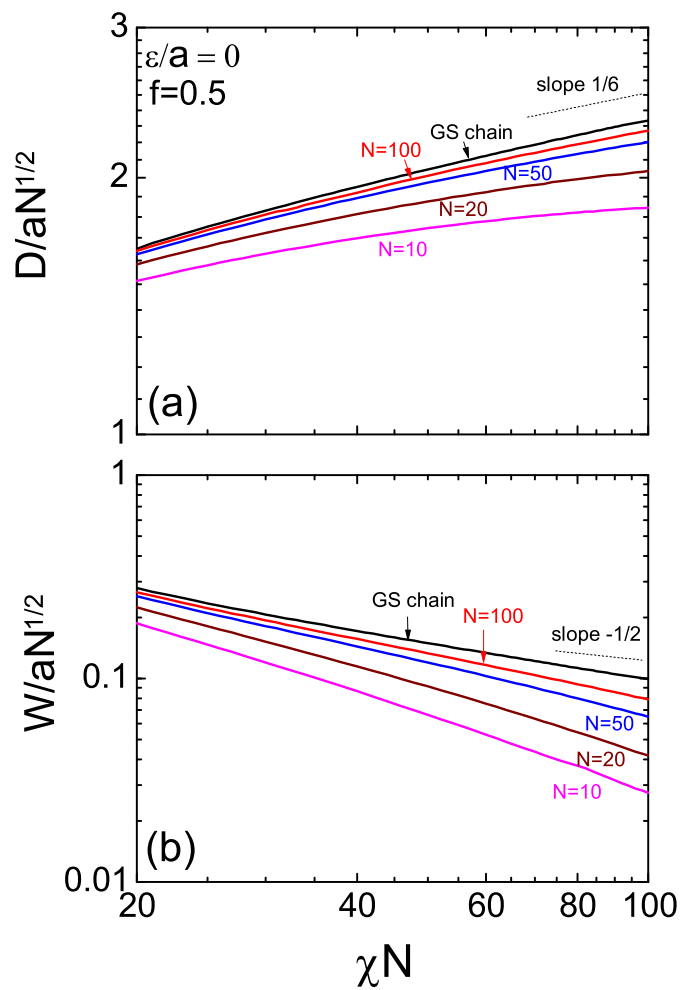
Figure 3: (a) Lamellar domain size *D* and (b) interfacial width *W* for symmetric AB diblock copolymers with $\varepsilon/a = 0$ as a function of χN in the strong-segregation regime. The dotted lines in (a) and (b) indicate the scaling behavior of $D \sim \chi^{1/6}$ and $W \sim \chi^{-1/2}$, respectively, predicted from GLC theory for large extremely large *N*.

(16), is suppressed by a $\tilde{h}(k)$ factor, where the latter is a decreasing function of $k\varepsilon$ [see Eqs. (17) and (18)]. Because of mixing-enthalpy suppression, the spinodal decomposition point $(\chi N)_s$ raises in a finite ε/a system in comparison with the ideal case.

Hence, the effects of finite interaction range on the spinodal decomposition can only be ignored on systems where $D \gg \varepsilon$. In low molecular systems with a moderate N, according to the wormlike chain model, D decreases much faster and becomes comparable to a. In a coarse-grained model where $\varepsilon \gtrsim a$, it becomes essential to consider the finite-ε/a effects because D is now comparable to ε.

III C. Deviation from the strong-segregation theory in low-molecular weight systems

As discussed above, for low-molecular systems, according to the current model, the important parameters that determine the properties of microphase separation are χN, f, N, and ε/a. For a symmetric, ordered system at $f = 1/2$ and beyond $(\chi N)_s$, in this subsection, we examine the effects of finite N on the properties of the microphase domain size and interfacial width as a function of χN, when the finite force range effects are ignored (i.e., $\varepsilon/a = 0$); the finite ε/a effects will be discussed in the next subsection. While the discussion in the last two subsections is based on RPA calculation, the analysis in the rest of the paper is based on a SCFT calculation that determines the spatially inhomogeneous and oriantationally ordered density profiles. The basic steps for such a calculation is presented in Appendix B.

At $f = 1/2$, the ordered structure is lamella. The symmetric diblock copolymers self-assemble into an ordered structure with one-dimensional spacial variation. There is a delicate balance between the entropy penalty of stretching the polymer chains and minimizing the interfacial tension, all together with the requirement of uniformly filling the available space. In comparison with a large N system which can be well-described by a GLC model, the finite N reduces chain entropy, enabling the system to make phase separation more easily.

The lamellar domain size D can be determined from minimizing the calculated SCFT free

energy per period. The interfacial width W for the symmetric lamellar phase is calculated from

$$W^{-1} = \left| \frac{\mathrm{d}\phi_A(z)}{\mathrm{d}z} \right|_{z=z_0} \tag{10}$$

where z_0 is the location of interface determined from $\phi_A(z_0) = \phi_B(z_0) = 1/2$.

Both D and W are plotted in Fig. 3 as a function of χN. The GSC model produces a single curve for all N (assumed large), plotted here as the black curve. In the large N limit, the curves asymptotically approach the scaling behavior

$$D/aN^{1/2} \propto (\chi N)^{1/6}, \tag{11}$$

and

$$W/aN^{1/2} \propto (\chi N)^{-1/2}, \tag{12}$$

in consistence with the prediction from the strong-segregation theory (SST);[35,36] such a theory is based on the assumption of strongly stretching a polymer chain, following the Gaussian chain statistics.

How much is the deviation of the properties of a finite-N system from these scaling power laws? The strong segregation regime is where the deviation becomes more transparent. The finite stretchability of a real polymer is suitably described by the non-stretchable WLC model used in this work. Fig. 3 shows that the finite-N effects become significant in systems where N is as large as 100. Both D and W curves no longer follow the ideal scaling power laws in (11) and (12) in a low molecular-weight system, such as $N = 10, 20, 50$.

Recently, Matsen studied SCFT of a diblock polymer system composed of FJCs.[27] The study depends on the number of bonds, N. The effects of finite N were examined in that work. In this model, a polymer is also unstretchable. He concludes that in the case of ignoring finite force-range effects, both D and W of small-N systems deviate from the ideal scaling laws. As χN increases and drives the system into the strongly segregation regime, the lamellar domain size approximately
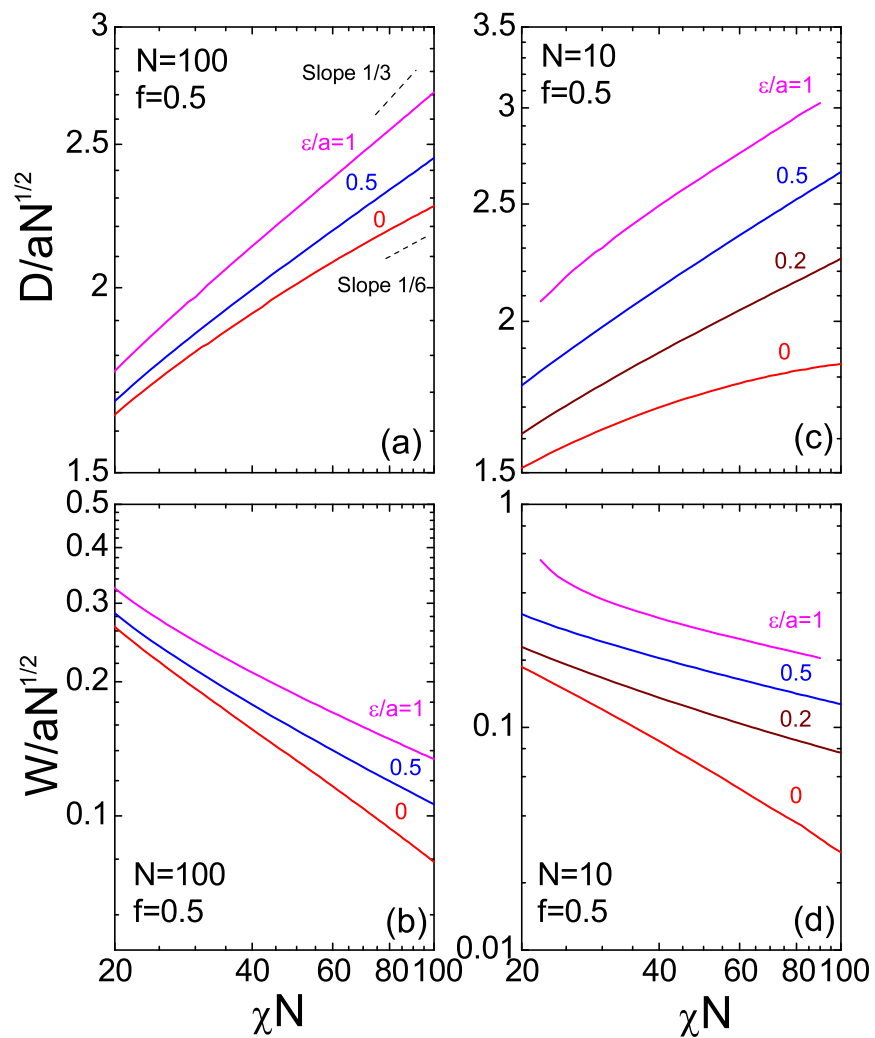
Figure 4: Domain size *D* and interfacial width *W* of the Lamellar phase for symmetric $N = 100$ [(a) and (b)] and $N = 10$ [(c) and (d)] AB diblock copolymers with various ε/a as functions of χN. The dashed lines represent the scaling power laws $D/a \sim \chi^{1/3}$ and $D/a \sim \chi^{1/6}$ in (a).

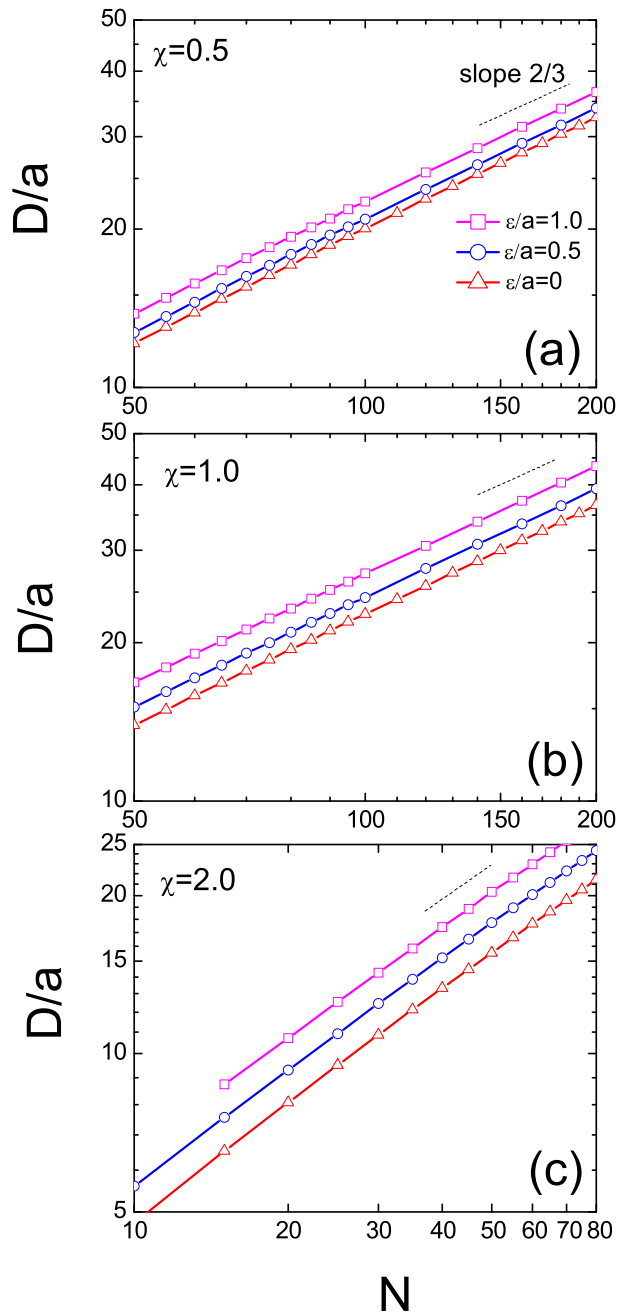Figure 5: Domain size *D* of the Lamellar phase for symmetric AB diblock copolymers with various ε/a as functions of *N* for (a) χ=0.5, (b) χ=1.0 and (c) χ=2.0. The dashed lines represent the scaling power law $D/a \sim N^{2/3}$.

follows the same scaling power in (11) until χN reaches 100 for $N = 40$, or χN reaches 300 for $N = 160$; the interfacial width, however, already dramatically decreases at a much smaller χN. This behavior is very different from that in our Fig. 3 where the deviations from the ideal scaling power laws of D and W happen not only at a much smaller χN, but in concert as well. In the strong segregation regime, the system runs into a small-W regime, which can be smaller than the Kuhn length a. The discrete features of the freely jointed chain model at that length scale is atypical of a real polymer. This can be contrasted to the approach taken in this paper; the wormlike chain model is able to capture the physical properties at a length scale below the Kuhn length. As illustrated in Fig. 3(b), our calculations indicate that at $\chi N = 100$, the interfacial width $W/a \simeq 0.085, 0.187,$ 0.458 and 0.789 for $N =$ 10, 20, 50 and 100, respectively.

III D. Properties of a finite-force-range theory in the strong-segregation regime

In the above we demonstrated that the ideal scaling power laws, Eqs. (11) and (12), as functions for both χ and N, break down in low-molecular weight systems where the finite force-range can be ignored, $\varepsilon/a = 0$. We now examine the effects of finite force range in the strong-segregation regime, represented by finite ε/a. The first case is $N = 100$, which, according to Fig. 3, approximately follows the ideal scaling law at large χN when $\varepsilon/a = 0$. This is re-plotted as the red curves in Fig. 4.

In a large-N system, are the ideal scaling laws for D/a and W/a valid within the strong-segregation regime as functions of χN and N in a system with finite force range? Our numerical results based on WLC theory, demonstrate a negative answer. The data shown in Figs. 4(a) and (b) for $N = 100$ indicate significant deviations of the χN-dependence from the ideal scaling laws. In the second case for $N = 10$ in Figs. 4(c) and (d), the entire behavior is different from the ideal scaling laws as well.

A different perspective, however, reveals an interesting property. Taking a few given ε/a, we show the numerical results based on wormlike-chain SCFT in Fig. 5 in double-logarithmic plots. For fixed χ, the results illustrate that the dependence of D/a on N still follows a power law that

can be characterized by the scaling exponent 2/3 predicted from SST over a wide range of N, even in the low molecular weight regime. A recent experiment measured the sub-5 nm domain size of a lamella state self-assembled from short diblock copolymers.[6] The D/a-N relation was shown to follow a power law behavior where a scaling exponent 0.68 was determined by fitting the experimental data. Our calculation in the above figure agrees with the general trend of D/a determined from this experiment.

How do we reconcile these different properties? A cross examination of plots in Figs. 4 and 5 suggests that within the parameter regime, an effective scaling behavior

$$D/a = A(\varepsilon/a, \chi) N^{2/3} \tag{13}$$

can be established in the strong-segregation regime. The function $A(\varepsilon/a, \chi)$ has the following properties

(a) When $\varepsilon/a = 0$ and $\chi \ll 1$, the prefactor $A(0, \chi)$ has the scaling behavior $\propto \chi^{1/6}$. An extremely large-N system, for example, are already in the lamella region. This is a case where the ideal scaling laws are recovered, as predicted by SST and verified here by data from wormlike-chain SCFT. Low-N systems are in the disorder phase region.

(b) When $\varepsilon/a = 0$ and $\chi \sim 1$, a moderate-N system can be phase separated into lamella state. The $\chi^{1/6}$ behavior breaks down. Hence, the ideal power laws are no longer followed by low-N systems.

(c) When $\varepsilon/a \sim 1$ and $\chi \gtrsim 1$, $A(1, \chi) \propto \chi^{1/3}$ as demonstrated by the numerical data in Fig. 4. The emergence of the exponent 1/3 in the latter case agrees with the exponent determined by Matsen for a lamellar domain size based on a SCFT of freely jointed chains.[27]

It would be interesting to more rigourously establish the scaling power law in Eq. (13) and determine the entire function $A(\varepsilon/a, \chi)$ from an analytical approach.
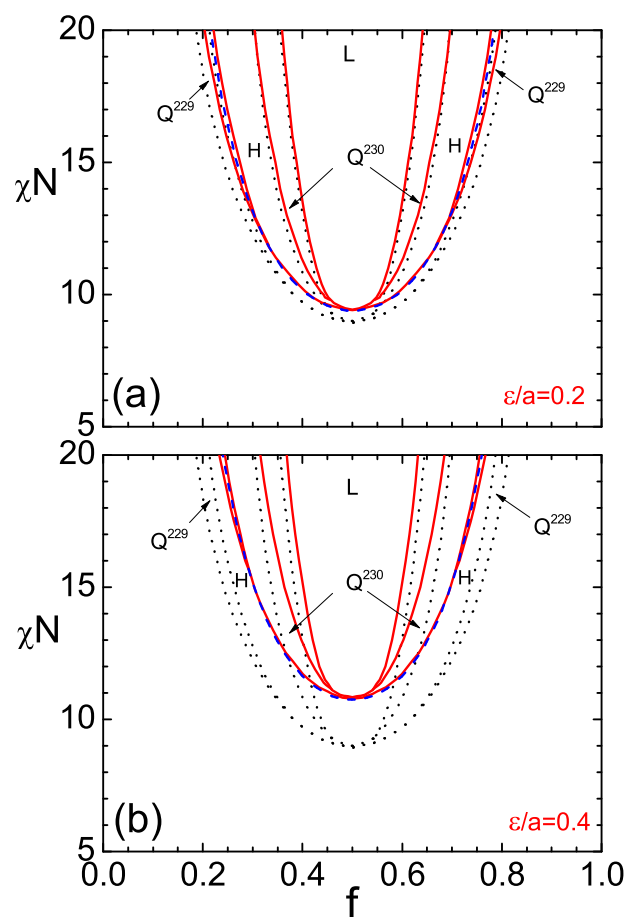
18

Figure 6: The phase diagram of symmetric $N = 10$ AB diblock copolymers for three interaction ranges: $\varepsilon/a = 0$ (dotted curves in both plots), $\varepsilon/a = 0.2$ [in (a)] and $\varepsilon/a = 0.4$ [in (b)]. The spinodal lines predicted from RPA for $\varepsilon/a = 0.2$ and $\varepsilon/a = 0.4$ are also labeled as dashed lines in (a) and (b), respectively. The stable regions for L (Lamellae), Q^{230} (bicontinuous gyroid), H (hexagonally ordered cylinder) and Q^{229} (body-centered sphere) are labeled in the diagrams.

III E. Phase diagram of a low-molecular weight system with finite force-range

The discussion so far is for a symmetric case where $f = 1/2$ and the ordered structure is lamella. Here we examine the effects of finite force range on a low-molecular weight system, $N = 10$, on the entire phase diagram. The SCFT calculation is performed based on Appendix B. The numerical scheme recently developed by two of us[25,26] is followed to determine the phase diagram, with, of course, an update to accommodate the nonlocal expressions for the mean fields in Eqs. (27) and (28).

The phase diagram for $\varepsilon/a = 0$ is plotted as dashed lines in Fig. 6. As discussed earlier, the entire ordered region is *shifted down*, characterized by an ODT point that is now shifted to $\chi N = 8.928...$ from $\chi N = 10.49....$[24] The basic structure of a diblock copolymer phase diagram is maintained: body-centered sphere (Q^{229}), hexagonally ordered cylinder (H), bicontinuous gyroid (Q^{230}), and lamellae (L), from a low f to $f = 1/2$.

The same figure shows the phase diagrams for systems with finite force range, $\varepsilon/a = 0.2$ and $\varepsilon/a = 0.4$. Consistent with our study based on RPA presented in Sect. III A, the stability region of all ordered states *shift up*. The ODT of the $\varepsilon/a = 0.4$ system has a value $\chi N = 10.84...$, greater than the ideal $\chi N = 10.49....$ The relative stability of morphologies is not changed fundamentally in these $\varepsilon/a \neq 0$ phase diagrams in comparison with the case $\varepsilon/a = 0$.

The present calculations only focus on the weak segregation regime where $\chi N \leq 20$. We expect more dramatic shifts of the phase boundaries in the strong segregation regime due to the sharp variation of the interfacial width; we demonstrated above the importance of both finite-N and finite ϵ/a effects. Unfortunately numerical data are currently unavailable in this parameter regime due to the increased computational cost needed to carry out the calculation for a sharp interface. As demonstrated in Fig. 4 (c), in the strong-segregation regime, wormlike diblock copolymers, owing to its inextensibility, is more easily stretched when a finite force range is explicitly involved. Consequently, a large energy penalty is demanded for the chain bending. Except for the lamellar phase, all other complex structures require bending of the polymer chains to meet the space filling requirement. Thus, we speculate that with finite force range, the lamellae is more preferred than

other structures in the strong-segregation regime.

IV. Summary

In the present work, using random-phase approximation and self-consistent field theory, we examine a number of effects, such as low-molecular weight and finite force range, on microphase separation of diblock copolymers in both weak and strong segregation regimes. The theoretical calculation is based on the wormlike chain model which can be used to describe a low-molecular weight system. A non-local demixing interaction energy between the two polymer components is considered; in such a form, a finite force range between polymer segments can be presented, beyond the local interaction energy that yields the Flory-Huggins interaction energy. The model reduces to a Gaussian-chain theory in the asymptotic limit of high-molecular weight.

Near the micro-phase separation boundary, our results reveal that the finite force effects are quite significant in modifying the order-disorder transition point (ODT) of low-molecular weight systems. This study substantiates the roles played by low-molecular weight polymers which prefers lowering ODT and played by finite force range which prefers raising ODT.

The structure of the phase diagram in the weak-to-moderate segregation regimes remains similar to the one determined from a Gaussian-chain based theory. In relation to the shift of ODT, the entire ordered phase regime move correspondingly in a low molecular-weight system where the polymers are still relatively flexible.

In the strong segregation regime, the interfacial width between the two unlike polymer domains, A-rich and B-rich, becomes extremely sharp. The study here uses the wormlike-chain model which is more realistic than the freely jointed chain model for sub-Kuhn-length physics; the interfacial properties demonstrated here, which are different from those derived from the free jointed chain model, can be used to facilitate a comparison with those determined from experimental studies.

Appendix A: Random phase approximation

In this section, we list the main steps of the random phase approximation (RPA) for the calculation of stability limit of the homogeneous (disorder) phase against a weak inhomogeneous condition.[40] This approach is based on the linear analysis of the disorder phase which can determine the spinodal line and the most instable fluctuation mode. For the wormlike-chain model, the central task is the calculation of the correlation function in the reciprocal space, as documented elsewhere.[24]

One can show that up to the quadratic order in density fluctuations, the partition function can be approximated by

$$Z \approx \exp(-\beta F^*) \int \mathcal{D}\{\delta\phi\} \exp\left\{-\beta F^{(2)}[\delta\phi]\right\}, \tag{14}$$

where F^* is the free energy at the mean-field level and $\delta\phi \equiv \delta\phi_A - \delta\phi_B$ is the volume-difference fluctuation. In $\mathbf{k}$-space, $F^{(2)}$ can be calculated from,[42]

$$\beta F^{(2)} = \frac{1}{2} \int \frac{d\mathbf{k}}{(2\pi)^3} \delta\phi(\mathbf{k}) C_{\text{RPA}}^{-1}(\mathbf{k}) \delta\phi(-\mathbf{k}), \tag{15}$$

where $C_{\text{RPA}}(\mathbf{k})$ is the $\mathbf{k}$ space representation of the RPA correlation function, i.e., the structure factor of the multi-chain system at the stability limit. The correlation function of the disorder state depends on modulus of the wavevector $k = |\mathbf{k}|$ only. For the current problem, it can be expressed in terms of the intrachain correlation functions C_{AA}, C_{BB} and C_{AB},

$$C_{\text{RPA}}^{-1}(k) \equiv \frac{C_{AA}(k) + 2C_{AB}(k) + C_{BB}(k)}{4\left[C_{AA}(k)C_{BB}(k) - C_{AB}^2(k)\right]} - \frac{1}{2}\chi N\tilde{h}(k), \tag{16}$$

where $\tilde{h}(k)$ is the Fourier transformation of the non-local kernel $h(\mathbf{r})$ discussed in Sect. II. For the wormlike-chain model, these correlation functions can be computed numerically following the method developed in Ref.[24]

Two specific examples of $h(\mathbf{r})$ are examined. We have

$$\tilde{h}_G(k) = \exp\left(-\frac{k^2 \varepsilon^2}{2}\right), \tag{17}$$

for the Gaussian function in Eq. (6) and

$$\tilde{h}_Y(k) = \frac{1}{k^2 \varepsilon^2 + 1}. \tag{18}$$

for the Yukawa function in Eq. (7). Once $C_{\mathrm{RPA}}^{-1}(k)$ is determined, we search for the minimum of this function numerically, which determines the soft mode k^*. As $C_{\mathrm{RPA}}^{-1}(k^*)$ approaches zero, the homogenous phase loses its stability. The spinodal point is determined from

$$(\chi N)_s = \min[\tilde{C}(k^*)/\tilde{h}(k^*)], \tag{19}$$

where

$$\tilde{C}(k) \equiv \frac{C_{AA}(k) + 2C_{AB}(k) + C_{BB}(k)}{2\left[C_{AA}(k)C_{BB}(k) - C_{AB}^2(k)\right]}. \tag{20}$$

The domain size of the order structure formed by microphase separation at ODT can be determined from

$$D \equiv 2\pi/k^*. \tag{21}$$

For both $\tilde{h}_G(k)$ and $\tilde{h}_Y(k)$ the results are shown in Sect. III A.

Appendix B: Self-consistent field theory of wormlike chains

A mean-field free energy can be established based on the basic theoretical framework introduced in Sect. II. The main steps are the same as those introduced in Refs.,[25,26] but now with the addition of the non-local enthalpic energy.

The partition function of the system is written as

$$Z = \frac{1}{n!} \int D\mathbf{R} \exp(-\beta\mathcal{H}_0 - \beta\mathcal{H}_1) \prod_{\mathbf{r}} \delta\left[1 - \hat{\phi}_A(\mathbf{r}) - \hat{\phi}_B(\mathbf{r})\right], \tag{22}$$

where a δ-function is introduced to represent the incompressibility condition. Taking the Hubbard-Stratonovich transformation,[28] we obtain the saddle-point approximation or the Helmholtz free energy per chain

$$\beta F = -\ln Q + \frac{1}{V} \int d\mathbf{r} \left[\chi N \int d\mathbf{r}' h(|\mathbf{r} - \mathbf{r}'|)\phi_A(\mathbf{r})\phi_B(\mathbf{r}') \right.$$
$$\left. - w_A(\mathbf{r})\phi_A(\mathbf{r}) - w_B(\mathbf{r})\phi_B(\mathbf{r}) + \xi(\mathbf{r})(\phi_A(\mathbf{r}) + \phi_B(\mathbf{r}) - 1) \right]. \tag{23}$$

which is a functional of the mean fields $w_A(\mathbf{r})$ and $w_B(\mathbf{r})$ that the A and B components experience, the volume fractions $\phi_A(\mathbf{r})$ and $\phi_B(\mathbf{r})$ at coordinate $\mathbf{r}$ which is already ensemble-averaged, and a Lagrangian multiplier $\xi(\mathbf{r})$ which enforces the incompressibility condition. The prefactor χN of the enthalpy term determines the magnitude of the demixing interaction. The single-chain partition function Q is calculated from

$$Q = \frac{1}{4\pi V} \int d\mathbf{r} d\mathbf{u} q(\mathbf{r}, \mathbf{u}, 1). \tag{24}$$

where $q(\mathbf{r}, \mathbf{u}, t)$ is a propagator.

The propagator $q(\mathbf{r}, \mathbf{u}, t)$ represents the probability of finding the end terminal, which is located at a spatial point specified by $\mathbf{r}$ and points in a direction specified by $\mathbf{u}$, of a polymer chain of contour length t. This function depends on the polymer model used to describe the statistical weight of a configuration. For a wormlike chain in an external field $w(\mathbf{r}, t)$, the propagator can be obtained from solving the modified diffusion equation (MDE)[28,43–45]

$$\frac{\partial}{\partial t} q(\mathbf{r}, \mathbf{u}, t) = \left[N\nabla_{\mathbf{u}}^2 - L\mathbf{u} \cdot \nabla_{\mathbf{r}} - w(\mathbf{r}, t) \right] q(\mathbf{r}, \mathbf{u}, t), \tag{25}$$

24

subject to the initial condition $q(\mathbf{r}, \mathbf{u}, 0) = 1$. In the current system,

$$w(\mathbf{r}, t) = \begin{cases} w_A(\mathbf{r}), & \text{if } 0 \le t \le f, \\ w_B(\mathbf{r}), & \text{if } f < t \le 1. \end{cases}$$

A complementary propagator $q^*(\mathbf{r}, \mathbf{u}, t)$ to $q(\mathbf{r}, \mathbf{u}, t)$ is needed to describe the probability of finding the end terminal, which is located at a spatial point specified by $\mathbf{r}$ and points in a direction specified by $-\mathbf{u}$, of a polymer chain of contour length $1 - t$. It satisfies a similar MDE

$$\frac{\partial}{\partial t} q^*(\mathbf{r}, \mathbf{u}, t) = \left[-N\nabla_{\mathbf{u}}^2 - L\mathbf{u} \cdot \nabla_{\mathbf{r}} + w(\mathbf{r}, t) \right] q^*(\mathbf{r}, \mathbf{u}, t), \tag{26}$$

and is subject to the initial condition $q^*(\mathbf{r}, \mathbf{u}, 1) = 1$ starting from the $t = 1$ terminal.

Minimization of the expression in Eq. (23) with respect to functions ϕ_A, ϕ_B, ξ, w_A and w_B provides a saddle-point solution of the free energy. We then obtain

$$w_A(\mathbf{r}) = \chi N \int d\mathbf{r}' h(\mathbf{r} - \mathbf{r}') \phi_B(\mathbf{r}) + \xi(\mathbf{r}), \tag{27}$$

$$w_B(\mathbf{r}) = \chi N \int d\mathbf{r}' h(\mathbf{r} - \mathbf{r}') \phi_A(\mathbf{r}) + \xi(\mathbf{r}), \tag{28}$$

$$\phi_A(\mathbf{r}) + \phi_B(\mathbf{r}) = 1, \tag{29}$$

$$\phi_A(\mathbf{r}) = \frac{1}{4\pi Q} \int d\mathbf{u} \int_0^f dt q(\mathbf{r}, \mathbf{u}, t) q^*(\mathbf{r}, \mathbf{u}, t), \tag{30}$$

and

$$\phi_B(\mathbf{r}) = \frac{1}{4\pi Q} \int d\mathbf{u} \int_f^1 dt q(\mathbf{r}, \mathbf{u}, t) q^*(\mathbf{r}, \mathbf{u}, t). \tag{31}$$

Equations (24) to (31) form a self-consistent set for the solution of the current problem.

Solving MDEs for both propagators $q(\mathbf{r}, \mathbf{u}, t)$ and $q^*(\mathbf{r}, \mathbf{u}, t)$ is a central task. These are functions simultaneously depending on three spatial variables to specify the vector $\mathbf{r}$, two orientational variables to specify the unit vector $\mathbf{u}$ and one time-like variable t. Various efforts[22,23,46–53] were made previously in designing numerical algorithms to solve Eqs. (25) and (26), for sys-

tems where the multi-dimensions can be reduced according to specific symmetries. To solve the full six-dimensional problem, a numerical algorithm has recently been introduced, based on a forward-backward scheme that incorporates spherical-harmonics expansion and Fourier transformation.[25,26] The current calculation is carried out by using this scheme.

Acknowledgments

References

(1) Bates, C. M.; Maher, M. J.; Janes, D. W.; Ellison, C. J.; Willson, C. G. *Macromolecules* **2014**, *47*, 2.

(2) Sinturel, C.; Bates, F. S.; Hillmyer, M. A. *ACS Macro Lett.* **2015**, *4*, 1044.

(3) Lee, S.; Gillard, T. M.; Bates, F. S. *AIChE J.* **2013**, *59*, 3502.

(4) Kim, S.; Nealey, P. F.; Bates, F. S. *Nano Lett.* **2013**, *14*, 148.

(5) Sweat, D. P.; Kim, M.; Larson, S. R.; Choi, J. W.; Choo, Y.; Osuji, C. O.; Gopalan, P. *Macromolecules* **2014**, *47*, 6687.

(6) Kennemur, J. G.; Yao, L.; Bates, F. S.; Hillmyer, M. A. *Macromolecules* **2014**, *47*, 1411.

(7) Luo, Y.; Montarnal, D.; Kim, S.; Shi, W.; Barteau, K. P.; Pester, C. W.; Hustad, P. D.; Christianson, M. D.; Fredrickson, G. H.; Kramer, E. J.; Hawker, C. J. *Macromolecules* **2015**, *48*, 3422.

(8) Schmid, F.; Schick, M. *J. Chem. Phys.* **1995**, *102*, 2080.

(9) Katsov, K.; Müller, M.; Schick, M. *Biophys. J.* **2004**, *87*, 3277.

(10) Thompson, R. B.; Jebb, T.; Wen, Y. *Soft Matter* **2012**, *8*, 9877.

(11) Hamley, I. W. *Nanotechnology* **2003**, *14*, R39.

(12) Tanner, P.; Baumann, P.; Enea, R.; Onaca, O.; Palivan, C.; Meier, W. *Acc. Chem. Res.* **2011**, *44*, 1039.

(13) Matsen, M. W.; Bates, F. S. *Macromolecules* **1996**, *29*, 1091.

(14) Cochran, E. W.; Garcia-Cervera, C. J.; Fredrickson, G. H. *Macromolecules* **2006**, *39*, 2449.

(15) Edwards, S. F. *Proc. Phys. Soc. London* **1965**, *85*, 613.

(16) Helfand, E. *J. Chem. Phys.* **1975**, *62*, 999.

(17) Fredrickson, G. H.; Ganesan, V.; Drolet, F. *Macromolecules* **2002**, *35*, 16.

(18) Matsen, M. W. *J. Phys.: Condens. Matter* **2002**, *14*, R21.

(19) Matsen, M. W. In *In Soft Matter: Polymer Melts and Mixtures*; Gompper, G., Schick, M., Eds.; Wiley-VCH: Weinheim, Germany, 2006; Vol. 1, Chapter 2.

(20) Kratky, O.; Porod, G. *Recl. Trav. Chim.* **1949**, *68*, 1106.

(21) Saito, N.; Takahashi, K.; Yunoki, Y. *J. Phys. Soc. Jpn* **1967**, *22*, 219.

(22) Matsen, M. W. *J. Chem. Phys.* **1996**, *104*, 7758.

(23) Jiang, Y.; Zhang, W.-Y.; Chen, J. Z. Y. *Physical Rev. E* **2011**, *84*, 041803.

(24) Zhang, X.; Jiang, Y.; Miao, B.; Chen, Y.; Yan, D.; Chen, J. Z. Y. *Soft Matter* **2014**, *10*, 5405.

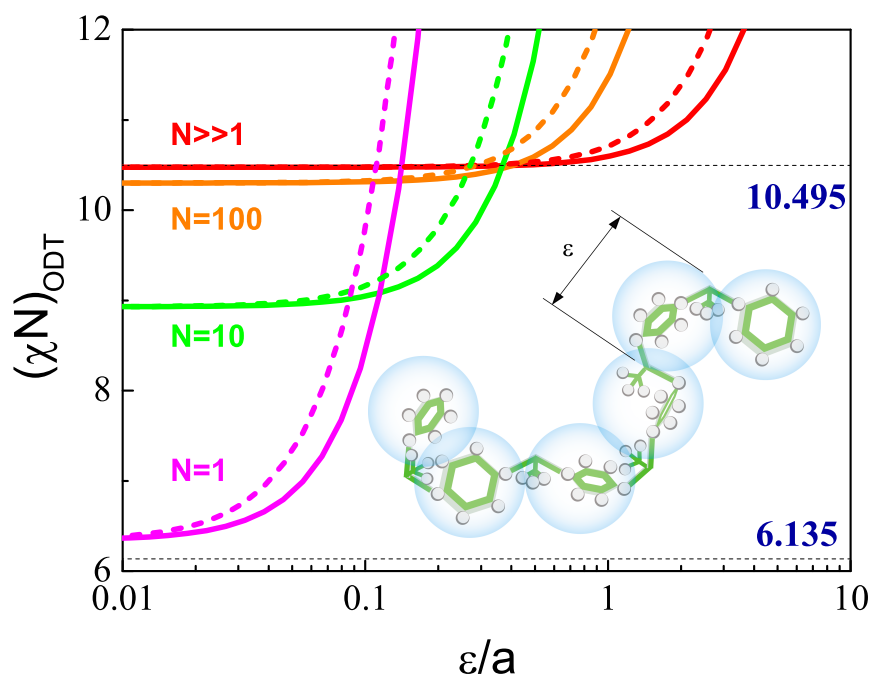(25) Jiang, Y.; Chen, J. Z. Y. *Physical Rev. E* **2013**, *88*, 042603.

(26) Jiang, Y.; Chen, J. Z. Y. *Phys. Rev. Lett.* **2013**, *110*, 138305.

(27) Matsen, M. W. *Macromolecules* **2012**, *45*, 8502.

(28) Fredrickson, G. H. *The Equilibrium Theory of Inhomogeneous Polymers*; Clarendon, Oxford, 2006.

(29) Wang, Z.-G. *Phys. Rev. E* **2010**, *81*, 021501.

(30) Alexander-Katz, A.; Moreira, A. G.; Sides, S. W.; Fredrickson, G. H. *J. Chem. Phys.* **2005**, *122*, 014904.

(31) Riggleman, R. A.; Kummar, R.; Fredrickson, G. H. *J. Chem. Phys.* **2012**, *136*, 024903.

(32) Koski, J.; Chao, H.; Riggleman, R. A. *J. Chem. Phys.* **2013**, *139*, 244911.

(33) Chao, H.; Hagberg, B. A.; Riggleman, R. A. *Soft Matter* **2014**, *40*, 8083.

(34) Villet, M. C.; Fredrickson, G. H. *J. Chem. Phys.* **2014**, *141*, 224115.

(35) Semenov, A. N. *Sov. Phys. JETP* **1985**, *61*, 733.

(36) Ohta, T.; Kawasaki, K. *Macromolecules* **1986**, *19*, 2621.

(37) Netz, R. R.; Orland, H. *Eur. Phys. J. B* **1999**, *8*, 81.

(38) Flory, P. J. *Principles of Polymer Chemistry*; Cornell University Press, Ithaca, 1953.

(39) Doi, M.; Edwards, S. F. *The Theory of Polymer Dynamics.*; Oxford Univ. Press, New York, 1986.

(40) Leibler, L. *Macromolecules* **1980**, *13*, 1602.

(41) Singh, C.; Goulian, M.; Andrea, J. L.; Fredrickson, G. H. *Macromolecules* **1994**, *27*, 2974.

(42) Shi, A.-C.; Noolandi, J.; Desai, R. D. *Macromolecules* **1996**, *29*, 6487.

(43) Freed, K. *Adv. Chem. Phys.* **1972**, *22*, 1.

(44) Liang, Q.; Li, J.-F.; Zhang, P.; Chen, J. Z. Y. *J. Chem. Phys.* **2013**, *138*, 244910.

(45) Chen, J. Z. Y. *Prog. Poly. Sci.* **2015**, *00*, 000.

(46) Cui, S.-M.; Akcakir, O.; Chen, Z. Y. *Phys. Rev. E* **1995**, *51*, 4548.

(47) Düchs, D.; Sullivan, D. E. *J. Phys.: Condens. Matter* **2002**, *14*, 12189.

(48) Song, W.; Tang, P.; Zhang, H.; Yang, Y.; Shi, A.-C. *Macromolecules* **2009**, *42*, 6300.

(49) Shah, M.; Ganesan, V. *J. Chem. Phys.* **2009**, *130*, 054904.

(50) Deng, M.; Jiang, Y.; Liang, H.; Chen, J. Z. Y. *Macromolecules* **2010**, *43*, 3455.

(51) Jiang, Y.; Chen, J. Z. Y. *Macromolecules* **2010**, *43*, 10668.

(52) Kumar, A.; Ganesan, V. *J. Chem. Phys.* **2012**, *136*, 101101.

(53) Gao, J.; Tang, P.; Yang, Y. *Soft Matter* **2013**, *9*, 69.

Table of Contents Graphic

Microphase separation of short wormlike diblock copolymers with finite interaction range
Ying Jiang, Xinghua Zhang, Bing Miao, Dadong Yan, and Jeff Z. Y. Chen

For Table of Contents Use Only